Structure of dysprosium and holmium phosphate glasses by the method of isomorphic substitution in neutron diffraction

2003 J. Phys.: Condens. Matter 15 8235

(http://iopscience.iop.org/0953-8984/15/49/003)

INSTITUTE OF PHYSICS PUBLISHING JOURNAL OF PHYSICS: CONDENSED MATTER

J. Phys.: Condens. Matter **15** (2003) 8235–8252 PII: S0953-8984(03)69718-3

Structure of dysprosium and holmium phosphate glasses by the method of isomorphic substitution in neutron diffraction

Richard A Martin[1], **Philip S Salmon**[1,4], **Henry E Fischer**[2] **and Gabriel J Cuello**[3]

[1] Department of Physics, University of Bath, Bath BA2 7AY, UK
[2] LURE, Centre Universitaire Paris-Sud, BP 34, F-91898, Orsay Cédex, France
[3] Institut Laue–Langevin, BP 156, F-38042, Grenoble Cédex 9, France

Received 28 September 2003
Published 25 November 2003
Online at stacks.iop.org/JPhysCM/15/8235

Abstract

The relative distribution of rare-earth ions R^{3+} (Dy^{3+} or Ho^{3+}) in the phosphate glass $RAl_{0.30}P_{3.05}O_{9.62}$ was measured by employing the method of isomorphic substitution in neutron diffraction and, by taking the role of Al into explicit account, a self-consistent model of the glass structure was developed. The glass network is found to be made from corner sharing PO_4 tetrahedra in which there are, on average, 2.32(9) terminal oxygen atoms, O_T, at 1.50(1) Å and 1.68(9) bridging oxygen atoms, O_B, at 1.60(1) Å. The network modifying R^{3+} ions bind to an average of 6.7(1) O_T and are distributed such that 7.9(7) R–R nearest neighbours reside at 5.62(6) Å. The Al^{3+} ion also has a network modifying role in which it helps to strengthen the glass through the formation of O_T–Al–O_T linkages. The connectivity of the R-centred coordination polyhedra in $(M_2O_3)_x(P_2O_5)_{1-x}$ glasses, where M^{3+} denotes a network modifying cation (R^{3+} or Al^{3+}), is quantified in terms of a parameter f_s. Methods for reducing the clustering of rare-earth ions in these materials are then discussed, based on a reduction of f_s via the replacement of R^{3+} by Al^{3+} at fixed total modifier content or via a change of x to increase the number of O_T available per network modifying M^{3+} cation.

1. Introduction

The incorporation of rare-earth ions, R^{3+}, into phosphate glasses confers these materials with many interesting opto-electronic and magneto-optical properties which give them application as, for example, lasers and Faraday rotators [1–7]. It is therefore desirable to understand the interactions between the rare-earth ions, and their mediation by the matrix material, in order

[4] Author to whom any correspondence should be addressed.

to develop non-phenomenological microscopic models. Hence progress is dependent on the provision of unambiguous experimental information about both the relative distribution of the rare-earth ions and the structure of the glassy matrix. This information can in principle be accessed, at the pair correlation function level, by means of diffraction methods through measurement of the so-called Faber–Ziman partial structure factors, $S_{\alpha\beta}(k)$, where k is the magnitude of the scattering vector [8]. The accompanying experimental challenge is, however, formidable. For instance, samples prepared by fusing RP_3O_9 in a platinum crucible comprise three chemical species and are described by six overlapping $S_{\alpha\beta}(k)$ [9]. Moreover, glasses with superior mechanical properties that enable fibres to be drawn, and which are also water resistant, can be prepared by fusing a suitable rare-earth oxide with P_2O_5 in an alumina crucible [10–12]. There is an attendant incorporation of Al into the structure [11] which further complicates the problem through the introduction of four additional $S_{\alpha\beta}(k)$. The literature on pair correlation functions in phosphate glasses, and in particular $S_{RR}(k)$, is therefore notable by its paucity.

In this paper, we tackle the problem by applying the method of *isomorphic* substitution in neutron diffraction to measure the R–R partial structure factor and related difference functions for the glassy phosphate $(R_2O_3)_{0.230}(Al_2O_3)_{0.069}(P_2O_5)_{0.701}$, or $RAl_{0.30}P_{3.05}O_{9.62}$, which contains *small* R^{3+} ions (Dy^{3+} or Ho^{3+}) from the heavy element end of the rare-earth series. The Dy^{3+} and Ho^{3+} ions were chosen as isomorphic pairs as they are adjacent in the periodic table and have comparable cation radii (0.912 cf 0.901 Å for sixfold coordination) [13] and Pettifor chemical parameters (0.685 cf 0.6825) [14]. They also share a similar structural chemistry [15, 16], e.g. the crystalline orthophosphates of the small rare-earth ions, c-RPO_4, have a common structure [17, 18]. Likewise, the crystalline metaphosphates, c-RP_3O_9, of the small rare-earth ions have a common structure [19], as do the crystalline ultraphosphates, c-RP_5O_{14} [20, 21].

From a practical point of view, the glasses contain a large mol% of rare-earth ions which enhances the prospect of identifying the R–R correlation. Furthermore, a variety of other techniques have been used to investigate the structure of similarly prepared R–Al–P–O glasses, including extended x-ray absorption fine structure (EXAFS) spectroscopy [22–27], neutron diffraction [11] and x-ray diffraction [12, 22, 28, 29]. Although trends associated with the lanthanide contraction [15, 16] have been observed, such as a shortening of the R–O nearest-neighbour distance, the R–R correlations have not been identified and significant differences in the structural parameters have been reported. For example, R–O coordination numbers in the range 5.8(6)–9.2(2.3) have been quoted for a glass with (nominal) composition $(Tb_2O_3)_{0.26}(P_2O_5)_{0.74}$ together with O–(P)–O coordination numbers in the range 3.4(3)–4.8(8) [11, 12, 22, 23, 25, 28], where the latter notation refers to oxygen atoms interlinked by phosphorus. Unambiguous information on these parameters is, however, of basic importance: the P–O and O–(P)–O peak positions and coordination numbers give insight into the connectivity of the phosphate network, through the ratio of bridging oxygen sites, O_B, to terminal oxygen sites, O_T, on the PO_4 tetrahedra, while the R–O coordination parameters help describe the degree of interlinking between R-centred polyhedra [9, 30–33]. A preliminary account of the present work on $RAl_{0.30}P_{3.05}O_{9.62}$ glasses is given elsewhere [34].

The essential theory required to understand the diffraction results will first be given in section 2. The sample preparation and characterization, together with the neutron diffraction method, will then be outlined in section 3. The results will be presented in section 4 and the steps taken to ensure the reliability of the measured $S_{RR}(k)$ and related difference functions will be explained. In the data analysis procedure, the structures of c-RP_3O_9 [19, 35] and c-RP_5O_{14} [21, 36] comprising *small* rare-earth cations will be used as a guide for interpreting the neutron diffraction results. Furthermore, *explicit* account will be taken of the Al correlations, by contrast with most previous diffraction and EXAFS studies in which the Al was regarded

as an impurity atom having a negligible impact on the measured patterns [11, 12, 22–28]. Finally, in section 5, the results for glassy $RAl_{0.30}P_{3.05}O_{9.62}$ will be discussed using the model of Hoppe and co-workers [9, 30–33] as a template and they will be compared with those recently obtained by applying the isomorphic substitution method in neutron diffraction to glassy $RAl_{0.35}P_{3.24}O_{10.12}$ [37], where R^{3+} denotes *large* cations (La^{3+} or Ce^{3+}) from the light element end of the rare-earth series. In particular, the connectivity of the R-centred coordination polyhedra in these two materials will be considered and methods for controlling the clustering of rare-earth ions in phosphate glasses will be discussed.

2. Theory

In a neutron diffraction experiment on an R–Al–P–O glass comprising a rare-earth paramagnetic cation, the differential scattering cross-section per atom for unpolarized neutrons can be written as

$$\left(\frac{d\sigma}{d\Omega}\right)_{tot} = \left(\frac{d\sigma}{d\Omega}\right)_{mag} + \left(\frac{d\sigma}{d\Omega}\right)_{nucl} \tag{1}$$

where $(d\sigma/d\Omega)_{mag}$ for Dy^{3+} or Ho^{3+} can be calculated in the free-ion approximation by using the scheme outlined in [38]. The nuclear differential scattering cross-section is given by

$$\left(\frac{d\sigma}{d\Omega}\right)_{nucl} = F(k) + \sum_{\alpha} c_\alpha [b_\alpha^2 + b_{inc,\alpha}^2][1 + P_\alpha(k)] \tag{2}$$

where the total structure factor is defined by

$$F(k) = \sum_{\alpha}\sum_{\beta} c_\alpha c_\beta b_\alpha b_\beta [S_{\alpha\beta}(k) - 1], \tag{3}$$

while c_α, b_α, $b_{inc,\alpha}$ and $P_\alpha(k)$ denote the atomic fraction, coherent scattering length, incoherent scattering length and inelasticity correction [39] for chemical species α. The accompanying real-space information is contained in the total pair correlation function $G(r)$ which is obtained from equation (3) by replacing the $S_{\alpha\beta}(k)$ by the corresponding partial pair distribution functions $g_{\alpha\beta}(r)$.

At the heart of the isomorphic substitution method, which has recently been used with success to study molten rare-earth compounds [38, 40–43], is the assumption that three glassy $RAl_{0.30}P_{3.05}O_{9.62}$ samples can be made that are structurally the same and differ only in the coherent neutron scattering length, b_R, of the rare-earth ion. If three total structure factors $F(k)$, $'F(k)$ and $''F(k)$ are measured corresponding to scattering lengths $b_R > b_{'R} > b_{''R}$ then those correlations not involving the rare-earth ion can be eliminated by subtracting two total structure factors to give a first-order difference function such as

$$\Delta F_R^{(1)}(k) \equiv F(k) - {}''F(k) = \Delta_{R\mu}^{(1)}(k) + c_R^2 \delta_R^{(1)} \varsigma_R^{(1)} [S_{RR}(k) - 1] \tag{4}$$

where μ (or μ') denotes a matrix atom (Al, P or O), $\delta_R^{(1)} = b_R - b_{''R}$, $\varsigma_R^{(1)} = b_R + b_{''R}$ and

$$\Delta_{R\mu}^{(1)}(k) = \sum_{\mu} 2 c_R c_\mu b_\mu \delta_R^{(1)} [S_{R\mu}(k) - 1]. \tag{5}$$

The other first-order difference functions are defined by $\Delta F_R^{(2)}(k) \equiv F(k) - {}' F(k)$ and $\Delta F_R^{(3)}(k) \equiv {}'F(k) - {}''F(k)$. It is then possible to eliminate the R–μ correlations by using, for instance, the combination [44, 45]

$$\begin{aligned} \Delta F^{(1)}(k) &\equiv F(k) - b_R \Delta F_R^{(1)}(k)/\delta_R^{(1)} \\ &= \Delta_{\mu\mu'}^{(1)}(k) - c_R^2 b_R b_{''R} [S_{RR}(k) - 1] \end{aligned} \tag{6}$$

where

$$\Delta^{(1)}_{\mu\mu'}(k) = \sum_{\mu}\sum_{\mu'} c_\mu c_{\mu'} b_\mu b_{\mu'}[S_{\mu\mu'}(k) - 1]. \tag{7}$$

Similarly, $\Delta F^{(2)}(k) \equiv F(k) - b_{\rm R}\Delta F^{(2)}_{\rm R}(k)/\delta^{(2)}_{\rm R}$ where $\delta^{(2)}_{\rm R} = b_{\rm R} - b_{'\rm R}$ and $\Delta F^{(3)}(k) \equiv {}'F(k) - b_{'\rm R}\Delta F^{(3)}_{\rm R}(k)/\delta^{(3)}_{\rm R}$ where $\delta^{(3)}_{\rm R} = b_{'\rm R} - b_{''\rm R}$.

The difference functions represented by equations (4) and (6) are particularly useful if only two structure factors are measured in an experiment [44]. However, the measurement of three total structure factors enables $S_{\rm RR}(k)$ to be extracted through the second-order difference function [45, 46]

$$S_{\rm RR}(k) - 1 = [(1-\gamma)F(k) - {}'F(k) + \gamma\,{}''F(k)][c^2_{\rm R}\gamma(1-\gamma)(\delta^{(1)}_{\rm R})^2]^{-1} \tag{8}$$

where $\gamma = \delta^{(2)}_{\rm R}/\delta^{(1)}_{\rm R}$ and $(1-\gamma) = \delta^{(3)}_{\rm R}/\delta^{(1)}_{\rm R}$ with $0 < \gamma < 1$. The R–μ correlations can then be isolated by the elimination of $S_{\rm RR}(k)$ from equation (4) to give equation (5) and the remaining functions $\Delta^{(2)}_{{\rm R}\mu}(k)$ and $\Delta^{(3)}_{{\rm R}\mu}(k)$ follow from similar expressions such that $\Delta^{(1)}_{{\rm R}\mu}(k)/\delta^{(1)}_{\rm R} = \Delta^{(2)}_{{\rm R}\mu}(k)/\delta^{(2)}_{\rm R} = \Delta^{(3)}_{{\rm R}\mu}(k)/\delta^{(3)}_{\rm R}$. The μ–μ' correlations can also be isolated by the elimination of $S_{\rm RR}(k)$ from equation (6) to give equation (7) and the remaining functions $\Delta^{(2)}_{\mu\mu'}(k)$ and $\Delta^{(3)}_{\mu\mu'}(k)$ follow from the elimination of $S_{\rm RR}(k)$ from $\Delta F^{(2)}(k)$ and $\Delta F^{(3)}(k)$ respectively such that all three $\Delta^{(i)}_{\mu\mu'}(k)$ $(i = 1, 2, 3)$ are identical. Hence the total structure factor $F(k)$ can be written as

$$F(k) = c^2_{\rm R}b^2_{\rm R}[S_{\rm RR}(k) - 1] + \frac{b_{\rm R}}{\delta^{(1)}_{\rm R}}\Delta^{(1)}_{{\rm R}\mu}(k) + \Delta^{(1)}_{\mu\mu'}(k) \tag{9}$$

which emphasizes its separation into a linear combination of the R–R, R–μ and μ–μ' correlation functions. The r-space representation of $S_{\rm RR}(k)$ is the partial pair distribution function $g_{\rm RR}(r)$ while the r-space representations of difference functions such as $\Delta^{(i)}_{{\rm R}\mu}(k)$ and $\Delta^{(i)}_{\mu\mu'}(k)$ $(i = 1, 2, 3)$ are denoted by $\Delta G^{(i)}_{{\rm R}\mu}(r)$ and $\Delta G^{(i)}_{\mu\mu'}(r)$ respectively and are obtained from the above equations for the k-space functions by replacing the $S_{\alpha\beta}(k)$ by the corresponding partial pair distribution function, $g_{\alpha\beta}(r)$. The limiting values of these functions, $\Delta G^{(i)}_{{\rm R}\mu}(0)$ and $\Delta G^{(i)}_{\mu\mu'}(0)$, follow from setting all of the $g_{\alpha\beta}(0) = 0$. The mean coordination number of β around α is denoted by $\bar{n}^{\beta}_{\alpha}$.

In practice, a measured total structure factor will be truncated by the finite measurement window of the diffractometer $M(k \leqslant k_{\rm max}) = 1, M(k > k_{\rm max}) = 0$ such that the accompanying r-space information is distorted by the modification function

$$M(r) = \frac{1}{\pi}\int_0^{k_{\rm max}} {\rm d}k\cos(kr) = \frac{1}{\pi r}\sin(k_{\rm max}r). \tag{10}$$

The difference functions are likewise modified and in order to gauge the extent of distortion it is useful to consider the r-space representation of the second-order difference function in the form

$$d'_{\rm RR}(r) = d_{\rm RR}(r) \otimes M(r), \tag{11}$$

where $d_{\rm RR}(r) = 4\pi n_0 r[g_{\rm RR}(r) - 1]$, n_0 is the atomic number density and $\otimes$ denotes the one-dimensional convolution operator. Useful r-space representations of the total pair correlation function and other main difference functions, in which the modification function retains its *symmetrical* form, are

$$D'(r) = \frac{4\pi n_0 r}{|G(0)|}G(r) \otimes M(r), \tag{12}$$

$$\Delta D'^{(i)}_{{\rm R}\mu}(r) = \frac{4\pi n_0 r}{|\Delta G^{(i)}_{{\rm R}\mu}(0)|}\Delta G^{(i)}_{{\rm R}\mu}(r) \otimes M(r), \tag{13}$$

and

$$\Delta D'^{(i)}_{\mu\mu'}(r) = \frac{4\pi n_0 r}{|\Delta G^{(i)}_{\mu\mu'}(0)|}\Delta G^{(i)}_{\mu\mu'}(r) \otimes M(r) \tag{14}$$

where the normalization of these functions, by $|G(0)|$, $|\Delta G^{(i)}_{\mathrm{R}\mu}(0)|$ and $|\Delta G^{(i)}_{\mu\mu'}(0)|$ respectively, ensures that the weighting factors of the $g_{\alpha\beta}(r)$ sum to unity such that the low-r limit in all cases is given by $-4\pi n_0 r$.

To enable those features that are an artifact of $M(r)$ to be distinguished, each peak j in $rg_{\alpha\beta}(r)$ can be represented by a Gaussian centred at $r_{\alpha\beta}(j)$ with standard deviation $\sigma_{\alpha\beta}(j)$ and area corresponding to a coordination number, $\bar{n}^{\beta}_{\alpha}(j)$, of species β around α. Then, for example, a measured R–μ difference function can be fitted by least squares to a sum of these Gaussians convoluted with $M(r)$ such that

$$\Delta D'^{(i)}_{\mathrm{R}\mu}(r) = \sum_j \left[\frac{W_{\alpha\beta}(j)\bar{n}^{\beta}_{\alpha}(j)}{\sqrt{2\pi}c_{\beta}(j)r_{\alpha\beta}(j)\sigma_{\alpha\beta}(j)} \exp\left(\frac{-(r - r_{\alpha\beta}(j))^2}{2\sigma^2_{\alpha\beta}(j)} \right) \otimes M(r) \right] - 4\pi n_0 r \tag{15}$$

where $W_{\alpha\beta}(j) = W_{\mathrm{R}\mu}(j) = 2c_{\mathrm{R}}c_{\mu}b_{\mu}\delta^{(i)}_{\mathrm{R}}/|\Delta G^{(i)}_{\mathrm{R}\mu}(0)|$. The right-hand side of equation (15) also holds for $d'_{\mathrm{RR}}(r)$, provided the $W_{\alpha\beta}(j)$ are set equal to unity, and for the $\Delta D'^{(i)}_{\mu\mu'}(r)$ difference functions, provided $W_{\alpha\beta}(j) = c^2_{\mu}b^2_{\mu}/|\Delta G^{(i)}_{\mu\mu'}(0)|$ if $\alpha = \beta = \mu$ and $W_{\alpha\beta}(j) = 2c_{\mu}c_{\mu'}b_{\mu}b_{\mu'}/|\Delta G^{(i)}_{\mu\mu'}(0)|$ if $\alpha(=\mu) \neq \beta(=\mu')$. In general, the peaks fitted at the larger r values are not expected to yield accurate parameters, owing to the overlap from correlations at even larger r, but are included to increase the reliability of the parameters that are reported for the peaks fitted at smaller r.

3. Experimental details

The three samples required for the diffraction experiments were made by fusing Dy_2O_3 (99.9%), Ho_2O_3 (99.9%) or an equal mixture of Dy_2O_3 and Ho_2O_3 with P_2O_5 (99%) in alumina (Al_2O_3) crucibles (Anderman). The dry oxide powders were mixed in an R_2O_3:P_2O_5 ratio of 0.15:0.85 which was chosen to ensure an excess of P_2O_5, relative to the metaphosphate composition $(R_2O_3)_{0.25}(P_2O_5)_{0.75}$, much of which sublimes during the glass preparation procedure. The powder mixtures (of mass $\approx$ 25 g) were initially allowed to absorb a fixed small amount ($\approx$100 mg) of atmospheric water at room temperature before the crucible with its lid were placed into a preheated oven at 500 °C for 1 h.[5] The crucible was then moved to another oven at 1000 °C, left for 30 min, and finally transferred to a third oven at 1680 °C. After 30 min the melt was poured into a preheated graphite mould and annealed at 500 °C for 24 h. The resultant glasses were transparent, free from bubbles and visibly homogeneous.

Although all of the glasses were prepared using an identical method, the crucibles were not sealed and the process by which the Al is incorporated into the glassy matrix is difficult to control. This precluded the use of expensive rare-earth isotopes and application of the *isotopic* substitution method in neutron diffraction [45–48]. Instead, it was necessary to prepare many samples and then select those with matching compositions, 1 R:0.30(3) Al:3.05(11) P:9.62(35) O, after investigation using electron probe micro-analysis. In the latter experiments, a cross-section was taken through each sample to examine the bulk material at several points and the glass composition was thereby found to be microscopically homogeneous. Factors aiding sample homogeneity are, presumably, the use of a small sample volume, which gives rise to a large contact area between the melt and crucible surface, and the fluidity of the melt at

[5] Test experiments indicate that a small initial water content helps to promote the formation of glassy materials.

Table 1. Weighting factors (in mbarn) for the $RAl_{0.30}P_{3.05}O_{9.62}$ glasses.

	$S_{RR}(k)$	$S_{RP}(k)$	$S_{RO}(k)$	$S_{RAl}(k)$	$S_{PP}(k)$	$S_{PO}(k)$	$S_{PAl}(k)$	$S_{OO}(k)$	$S_{AlO}(k)$	$S_{AlAl}(k)$
$^{Dy}F(k)$	13.2(3)	25.6(3)	91.7(1.1)	1.70(2)	12.51(5)	89.4(2)	1.656(4)	159.8(2)	5.919(10)	0.0548(2)
$^{mix}F(k)$	7.5(1)	19.3(2)	69.1(6)	1.28(1)	12.51(5)	89.4(2)	1.656(4)	159.8(2)	5.919(10)	0.0548(2)
$^{Ho}F(k)$	3.29(7)	12.8(1)	45.8(5)	0.849(9)	12.51(5)	89.4(2)	1.656(4)	159.8(2)	5.919(10)	0.0548(2)
$\Delta F_R^{(1)}(k)$	9.9(3)	12.8(3)	45.8(1.2)	0.85(2)	—	—	—	—	—	—
$\Delta F_R^{(2)}(k)$	5.7(4)	6.3(4)	22.6(1.3)	0.42(2)	—	—	—	—	—	—
$\Delta F_R^{(3)}(k)$	4.2(2)	6.5(2)	23.2(8)	0.43(1)	—	—	—	—	—	—
$\Delta_{R\mu}^{(1)}(k)$	—	12.8(3)	45.8(1.2)	0.85(2)	—	—	—	—	—	—
$\Delta F^{(1)}(k)$	−6.6(1.4)	—	—	—	12.51(5)	89.4(2)	1.656(4)	159.8(2)	5.919(10)	0.0548(2)
$\Delta F^{(2)}(k)$	−9.9(1.5)	—	—	—	12.51(5)	89.4(2)	1.656(4)	159.8(2)	5.919(10)	0.0548(2)
$\Delta F^{(3)}(k)$	−4.95(6)	—	—	—	12.51(5)	89.4(2)	1.656(4)	159.8(2)	5.919(10)	0.0548(2)
$\Delta_{\mu\mu'}^{(1)}(k)$	—	—	—	—	12.51(5)	89.4(2)	1.656(4)	159.8(2)	5.919(10)	0.0548(2)

the high temperatures utilized, which helps to distribute the alumina dissolved at the crucible surface throughout the bulk material. It was found that, by comparison with phosphate glasses containing large rare-earth cations [37, 49], a relatively small distribution of compositions resulted. The mass density was determined by measuring the sample weight in fluids of different density and $n_0 = 0.0715(6)$ Å^{-3} was thereby deduced for each of the glasses.

The neutron diffraction experiments were performed using the D4C instrument at the Institut Laue–Langevin (Grenoble) with an incident neutron wavelength of 0.7100 Å [50, 51]. The coarsely powdered samples were held at ambient temperature (≈25 °C) in a cylindrical vanadium can of 4.8 mm internal diameter and 0.1 mm wall thickness and diffraction patterns were taken for the samples in their container, the empty container and a vanadium rod of dimensions comparable to the sample for normalization purposes. The intensity for a cadmium neutron-absorbing rod of similar diameter to the sample was also measured to account for the effect of sample self-shielding on the background count rate at small scattering angles [52]. Each complete diffraction pattern was built up from the intensities measured for the different detector groups. These intensities were saved at regular intervals and no deviation between them was observed, apart from the expected statistical variations, which verified the diffractometer stability [50, 51, 53]. The total paramagnetic scattering cross-sections of Dy^{3+} and Ho^{3+} at the incident neutron wavelength were calculated using the method given in [38]. The coherent neutron scattering lengths $b_{Ho} = 8.01(8)$, $b_{Al} = 3.449(5)$, $b_P = 5.13(1)$ and $b_O = 5.803(4)$ fm were taken from Sears [54]. For thermal neutrons, however, resonance effects make the scattering length of ^{164}Dy sensitive to the incident neutron energy [55]. Breit–Wigner theory [56] was therefore used to modify the ^{164}Dy coherent scattering length from 49.4(2) fm for 1.798 Å wavelength neutrons [54] to 46.3(2) fm for 0.71 Å wavelength neutrons, taking into account a resonance for ^{164}Dy at −1.88 eV [57]. An overall Dy scattering length $b_{Dy} = 16.0(2)$ fm was thereby deduced compared with a value of 16.9(2) fm at 1.798 Å [54]. The weighting factors for the $S_{\alpha\beta}(k)$ appearing in the various formulae are given in table 1 and $\Delta_{R\mu}^{(1)}(k) = 2.03\ \Delta_{R\mu}^{(2)}(k) = 1.97\ \Delta_{R\mu}^{(3)}(k)$ while $\Delta_{\mu\mu'}^{(1)}(k) = \Delta_{\mu\mu'}^{(2)}(k) = \Delta_{\mu\mu'}^{(3)}(k)$.

At each stage of the data analysis procedure, described in [45], a full set of reliability checks was performed to test the efficacy of the isomorphic assumption. For example, each measured difference function should obey the usual sum-rule relation and give rise to a well behaved real-space function: this should oscillate about the calculated low-r limit and, when the oscillations are set to this limit, its back Fourier transform should be in good overall agreement with the original reciprocal space data set. Furthermore, as three different routes may be used

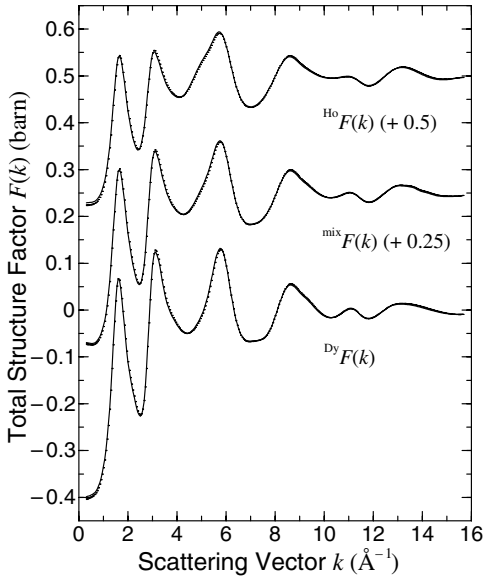

Figure 1. The measured total structure factors $^{Dy}F(k)$, $^{mix}F(k)$ and $^{Ho}F(k)$ for glassy $RAl_{0.30}P_{3.05}O_{9.62}$. The data are represented by the points with error bars and the solid curves are the back Fourier transforms of the corresponding $D'(r)$ after the unphysical low-r oscillations are set to the calculated limit of $-4\pi n_0 r$ (see figure 2). The back Fourier transforms are almost indistinguishable from the data points on the plot scale at most k values.

to construct the experimental difference functions, the three $\Delta^{(i)}_{R\mu}(k)/\delta^{(i)}_{R}$ $(i = 1, 2, 3)$ should be the same within the statistical uncertainties and, likewise, the three $\Delta^{(i)}_{\mu\mu'}(k)$ $(i = 1, 2, 3)$.

4. Results

The measured total structure factors are shown in figure 1 and are denoted by $^{Dy}F(k)$, $^{mix}F(k)$ and $^{Ho}F(k)$ where 'mix' denotes a 1:0.97 mixture of Dy and Ho and $b_{Dy} > b_{mix} > b_{Ho}$. There is good overall agreement between each $F(k)$ and the back Fourier transform of the corresponding total pair correlation function $D'(r)$, after the unphysical low-r oscillations are set to their calculated limit of $-4\pi n_0 r$ (see figure 2), which indicates that the data correction procedures have been properly applied [45]. The total structure factors show a clear contrast in signal as demonstrated by the difference functions $\Delta F^{(i)}_{R}(k)$ and $\Delta F^{(i)}(k)$ $(i = 1, 2, 3)$ illustrated in figure 3. The three $\Delta F^{(i)}_{R}(k)$ have distinct features at smaller k values that can be attributed to the $S_{RR}(k)$ partial structure factor: unlike the weighting factor for $S_{RR}(k)$ in the expression for $\Delta F^{(i)}_{R}(k)$, the weighting factors for the R–μ correlations have the same relative ratio in each function (see table 1). The measured $\Delta F^{(i)}(k)$ also have distinct features that can be attributed to $S_{RR}(k)$ as the weighting factors for the μ–μ' correlations are identical in all three functions.

The measured total structure factors, represented by the error bars in figure 1, were used in equation (8) to extract the partial structure factor $S_{RR}(k)$ shown in figure 4. The high-k oscillations of this function are heavily damped which implies that the effect of the modification function will be small, i.e. we will take $d'_{RR}(r) = d_{RR}(r)$ in the following discussion. The dominant features in $S_{RR}(k)$ are two peaks at low k which motivated a smooth truncation of the data, by application of a cosine window function over the region $4 \leqslant k$ (Å^{-1}) $\leqslant 5$ prior

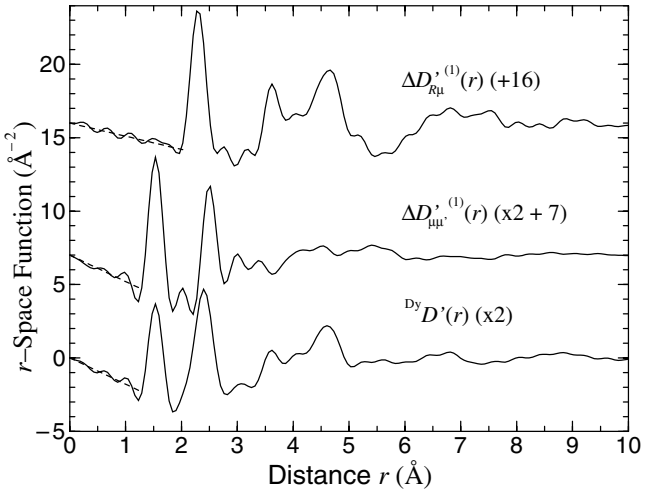

Figure 2. The total pair correlation function $D'(r)$ for glassy $DyAl_{0.30}P_{3.05}O_{9.62}$, obtained by Fourier transforming the total structure factor $^{Dy}F(k)$ given by the points with error bars in figure 1, together with the difference functions $\Delta D'^{(1)}_{R\mu}(r)$ and $\Delta D'^{(1)}_{\mu\mu'}(r)$, obtained by Fourier transforming the difference functions $\Delta^{(1)}_{R\mu}(k)$ and $\Delta^{(1)}_{\mu\mu'}(k)$ given by the points with error bars in figures 6 and 7 respectively. The calculated low-r limit of all these functions is equal to $-4\pi n_0 r$ and is shown by the dashed curves.

to Fourier transformation, in order to identify the corresponding main features in r space. The resultant pair correlation function $d_{RR}(r)$, shown in figure 5(a), has a first peak at 5.65(2) Å giving $\bar{n}^R_R = 8.6(2)$ with no clearly identifiable features at lower r. Next, the entire k-space range of $S_{RR}(k)$ was transformed and the resultant $d_{RR}(r)$ also shows a strong peak at a comparable position of 5.55(2) Å giving $\bar{n}^R_R = 7.9(2)$. More pronounced features are observed at lower r but these could not be definitively identified with unwanted correlations (cf [48]): for example, when the oscillations for $0 \leqslant r$ (Å) $\leqslant 5.1$ (including the peak at 4.72 Å) are set to the low-r limit of $-4\pi n_0 r$ and the data are back Fourier transformed the resultant function is in reasonable agreement with the measured $S_{RR}(k)$ over the entire k-space range (figure 4). Finally, the minimum-noise reconstruction method was used [58], which gives, essentially, a smooth $d_{RR}(r)$ that is constrained to take physical values, i.e. $d_{RR}(r) = -4\pi n_0 r$ for $0 \leqslant r \leqslant r_{min}$ and $d_{RR}(r) \geqslant -4\pi n_0 r$ for $r > r_{min}$, with r_{min} varied between 4.5 and 5.1 Å. A first peak at 5.65(2) Å was obtained, with $\bar{n}^R_R = 7.2(2)$, and no physical features could be generated for $4.5 \leqslant r$ (Å) $\leqslant 5.1$. Thus, the diffraction data identify a first-nearest-neighbour R–R distance of 5.62(6) Å with $\bar{n}^R_R = 7.9(7)$ together with *intermediate*-range ordering of the R–R correlations extending beyond 15 Å (figure 5(a)). This picture is consistent with the structure of c-RP_3O_9, in which eight nearest-neighbour R–R ions reside in the range 5.4–7.0 Å [35], and the absence of R–R correlations at $r \leqslant 4$ Å is in accord with other studies [7, 11, 12, 25, 26]. The observed R–R nearest-neighbour distance of 5.62(6) Å in the glass compares with a value of 5.80 Å expected from a uniform distribution of R^{3+} ions in which their separation is maximized.

The $\Delta^{(i)}_{R\mu}(k)$ ($i = 1, 2, 3$) are shown in figure 6 and were extracted from the first-order difference functions $\Delta F^{(i)}_R(k)$ by using equation (4) with $S_{RR}(k)$ taken from the solid curve in figure 4. Unlike the $\Delta F^{(i)}_R(k)$ (see figure 3(a)), the $\Delta^{(i)}_{R\mu}(k)/\delta^{(i)}_R$ are comparable within the statistical uncertainties, as indicated by the differences $[\Delta^{(1)}_{R\mu}(k) - 2.03\Delta^{(2)}_{R\mu}(k)]$

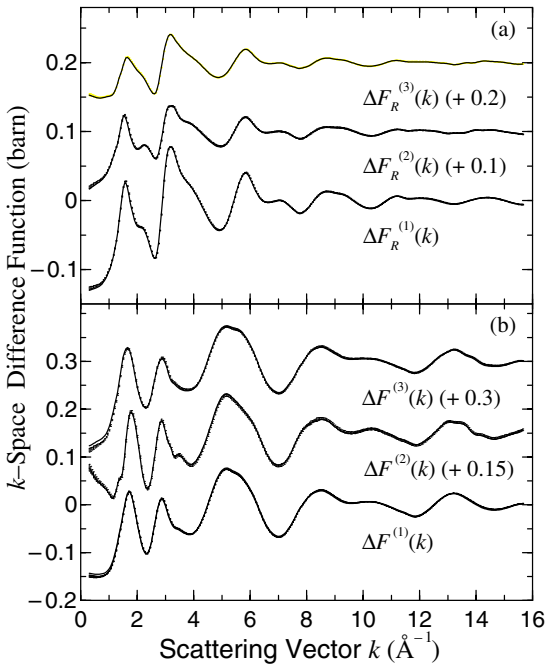

Figure 3. The measured difference functions (a) $\Delta F_{\mathrm{R}}^{(i)}(k)$ and (b) $\Delta F^{(i)}(k)$ for glassy $\mathrm{RAl_{0.30}P_{3.05}O_{9.62}}$ obtained from the total structure factors given in figure 1 by using equations (4) and (6) respectively. The data are represented by the points with error bars and the solid curves are the back Fourier transforms of the corresponding r-space functions after the unphysical low-r oscillations are set to the calculated limit of $-4\pi n_0 r$. The back Fourier transforms are almost indistinguishable from the data points on the plot scale at most k values. Each set of curves for $\Delta F_{\mathrm{R}}^{(i)}(k)$ $(i = 1, 2, 3)$ or $\Delta F^{(i)}(k)$ $(i = 1, 2, 3)$ has contrasting features that are most noticeable at smaller k values and which can be attributed to the presence with different weighting factors of the $S_{\mathrm{RR}}(k)$ partial structure factor (see the text).

and $[\Delta_{\mathrm{R}\mu}^{(1)}(k) - 1.97\Delta_{\mathrm{R}\mu}^{(3)}(k)]$, which points to a correct data analysis procedure [45]. The r-space function $\Delta D_{\mathrm{R}\mu}^{\prime\,(1)}(r)$, obtained by direct Fourier transformation of $\Delta_{\mathrm{R}\mu}^{(1)}(k)$, is shown in figure 2. For c-$\mathrm{ErP_3O_9}$ the shortest R–O, R–(O)–P and R–R distances are 2.17, 3.49 and 5.37 Å respectively and the second-nearest-neighbour R–O distance is 3.83 Å [35], where R–(O)–P denotes R and P interlinked by O. The corresponding distances are 2.29, 3.60, 5.71 and 3.99 Å for c-$\mathrm{HoP_5O_{14}}$ [36] and 2.31, 3.01, 3.75 and 4.14 Å for c-$\mathrm{HoPO_4}$ [18]. Hence only R–O correlations are expected for $r \leqslant 3$ Å and the first peak in $\Delta D_{\mathrm{R}\mu}^{\prime\,(1)}(r)$ at 2.27 Å was identified with R–O correlations and the second peak at 3.62 Å with R–(O)–P correlations. To take into account the effect of the modification function $M(r)$, the data were fitted over the range $2.0 \leqslant r$ (Å) $\leqslant 3.4$ by using equation (15) and the results are shown in figure 5(b). The procedure gave a goodness-of-fit parameter R_χ [59] of 1.3% and yielded nearest-neighbour Gaussians corresponding to $\bar{n}_{\mathrm{R}}^{\mathrm{O}} = 6.2(1)$ at 2.30(1) Å and $\bar{n}_{\mathrm{R}}^{\mathrm{O}} = 0.5(1)$ at 2.67(1) Å. The results therefore show an $\mathrm{R^{3+}}$ ion coordination environment that is distorted relative to c-$\mathrm{RP_3O_9}$, in which six R–O neighbours reside in the range $2.17 \leqslant r$ (Å) $\leqslant 2.29$ [35], and the overall coordination number $\bar{n}_{\mathrm{R}}^{\mathrm{O}} = 6.7(1)$ in the glass compares with $\bar{n}_{\mathrm{R}}^{\mathrm{O}} = 8$ for $2.29 \leqslant r$ (Å) $\leqslant 2.41$ in c-$\mathrm{RP_5O_{14}}$ [36].

The full set of parameters describing the Gaussians fitted to $\Delta D_{\mathrm{R}\mu}^{\prime\,(1)}(r)$ is given in table 2. Within the experimental error, these are the same as the parameters obtained by

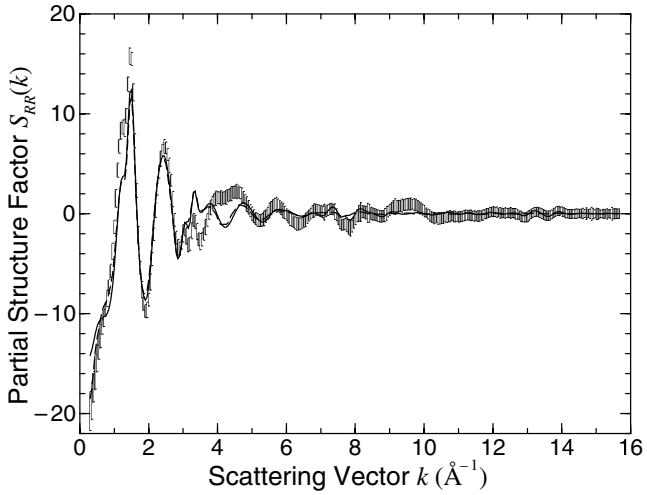

Figure 4. The partial structure factor $S_{\mathrm{RR}}(k)$ for glassy $\mathrm{RAl_{0.30}P_{3.05}O_{9.62}}$ obtained from the total structure factors given in figure 1 by use of equation (8). The measured data are represented by the points with error bars while the dashed curve gives the minimum noise solution and the solid curve gives the back Fourier transform of $d_{\mathrm{RR}}(r)$ shown by the circles in figure 5(a) after the unphysical low-r oscillations are set to the calculated limit of $-4\pi n_0 r$.

Table 2. Parameters obtained from the Gaussian fit to the $\Delta D'^{(1)}_{\mathrm{R}\mu}(r)$ difference function for glassy $\mathrm{RAl_{0.30}P_{3.05}O_{9.62}}$.

Correlation (α–β)	$r_{\alpha\beta}$ (Å)	$\bar{n}^{\beta}_{\alpha}$	$\sigma_{\alpha\beta}$ (Å)
R–O	2.30(1)	6.2(1)	0.11(1)
R–O	2.67(2)	0.5(1)	0.11(1)
R–(O)–P	3.25(2)	1.1(2)	0.11(2)
R–(O)–P	3.60(2)	6.0(2)	0.10(2)

fitting $\Delta D'^{(2)}_{\mathrm{R}\mu}(r)$ and $\Delta D'^{(3)}_{\mathrm{R}\mu}(r)$, i.e. no change in the first-nearest-neighbour R–O distance was found that could be attributed to a difference of 0.011 Å between the radii of Dy^{3+} and Ho^{3+} [13]. Although a small systematic increase of the first-nearest-neighbour R–O distance with increasing cation radius was observed when fitting the $D'(r)$ functions, the change was within the error of ± 0.01 Å on a peak position. Hence, diffraction data extending to high k values that give enhanced r-space resolution would be required to identify any effects that arise from the lanthanide contraction [15, 16].

The $\Delta^{(i)}_{\mu\mu'}(k)$ ($i = 1, 2, 3$) are shown in figure 7 and were extracted from the $\Delta F^{(i)}(k)$ by using equation (6) with $S_{\mathrm{RR}}(k)$ taken from the solid curve in figure 4. Unlike the $\Delta F^{(i)}(k)$ (see figure 3(b)), the $\Delta^{(i)}_{\mu\mu'}(k)$ are comparable within the statistical uncertainties, as indicated by the differences $[\Delta^{(1)}_{\mu\mu'}(k) - \Delta^{(2)}_{\mu\mu'}(k)]$ and $[\Delta^{(1)}_{\mu\mu'}(k) - \Delta^{(3)}_{\mu\mu'}(k)]$, which points to the absence of any substantial systematic error [45]. The r-space function $\Delta D'^{(1)}_{\mu\mu'}(r)$, obtained by direct Fourier transformation of $\Delta^{(1)}_{\mu\mu'}(k)$, is shown in figure 2. In c-ErP_3O_9 the shortest P–O, O–(P)–O and P–(O)–P distances are 1.40, 2.32 and 2.89 Å respectively [35], where O–(P)–O denotes oxygen atoms interlinked by phosphorus and P–(O)–P denotes phosphorus atoms interlinked by O, and the corresponding distances are 1.44, 2.38 and 2.86 Å for c-HoP_5O_{14} [36]. In c-$HoPO_4$, the PO_4 units are isolated and the shortest P–O, O–(P)–O

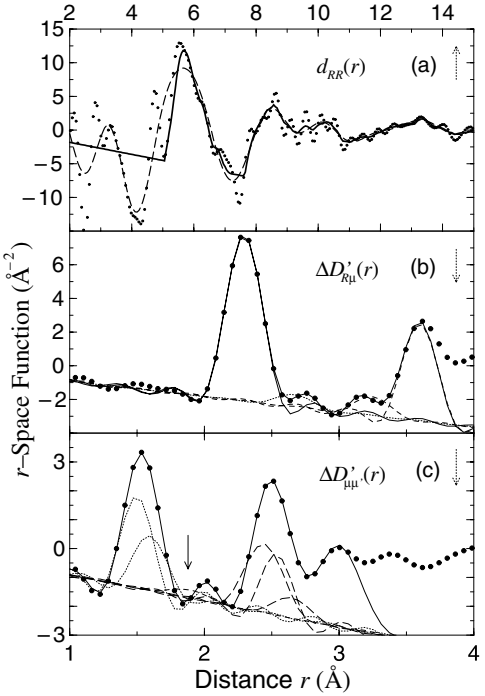

Figure 5. The circles give the real-space functions (a) $d_{RR}(r)$, (b) $\Delta D'^{(1)}_{R\mu}(r)$ and (c) $\Delta D'^{(1)}_{\mu\mu'}(r)$ obtained by Fourier transforming the reciprocal space functions shown in (a) figure 4, (b) figure 6 and (c) figure 7 respectively. The dotted arrows point to the relevant abscissa scale. In (a) the solid curve gives the minimum information solution and the dashed curve shows the effect of smoothly truncating $S_{RR}(k)$ by using a cosine function. In (b) and (c), the solid curves give the fitted function and the other curves the individual convoluted Gaussians: in (b) R–O (dotted curves) and R–P (dashed curves); in (c) P–O (dotted curves), Al–O (dashed curve) and O–O (long-dashed curves). Several of the larger-r Gaussians are omitted from (c) for clarity of presentation. The solid arrow in (c) points to the Al–O Gaussian peak position.

and P–P distances are 1.53, 2.40 and 3.75 Å respectively [18]. The first peak in $\Delta D'^{(1)}_{\mu\mu'}(r)$ at 1.53(2) Å was therefore assigned to the P–O correlations from PO_4 tetrahedra and the corresponding O–(P)–O correlations will give a strong contribution to the second peak at 2.52(2) Å. The region between these two peaks, $1.7 \leqslant r$ (Å) $\leqslant 1.9$, will have a contribution from Al–O correlations since ^{27}Al nuclear magnetic resonance experiments, made on rare-earth phosphate glasses prepared in alumina crucibles [11], show that Al can be fourfold, fivefold or sixfold coordinated to oxygen. In c-AlP_3O_9 [60], aluminium is octahedrally coordinated to oxygen at a distance $r_{AlO} = 1.88$ Å giving an O–(Al)–O nearest-neighbour separation of $\sqrt{2}r_{AlO} = 2.66$ Å, placing these correlations under the second peak in $\Delta D'^{(1)}_{\mu\mu'}(r)$. By comparison, for tetrahedral coordination $r_{AlO} = 1.76$ Å [61], giving an O–(Al)–O distance of $\sqrt{8/3}r_{AlO} = 2.87$ Å in the region between the second and third peaks in $\Delta D'^{(1)}_{\mu\mu'}(r)$. The second peak has, therefore, contributions *only* from O–(P)–O and O–(Al)–O correlations whilst the third peak was modelled assuming P–(OP)–O, P–(O)–P, O–(R)–O and Al–(O)–P correlations using the structures of c-RP_3O_9 [19, 35] and c-AlP_3O_9 [60] as starting points.

As detailed in section 2, a Gaussian fit to $\Delta D'^{(1)}_{\mu\mu'}(r)$ taking into account the effect of the modification function, $M(r)$, was made over the range $1.2 \leqslant r$ (Å) $\leqslant 2.9$ and gave $R_\chi = 2.0\%$

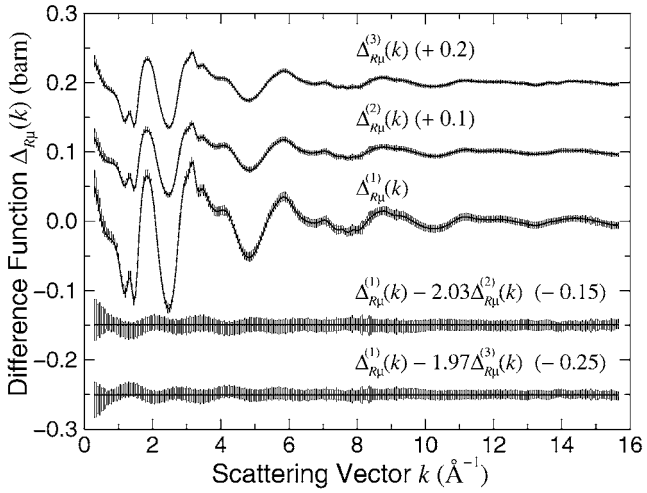

Figure 6. The R-matrix atom difference functions $\Delta^{(i)}_{R\mu}(k)$ $(i = 1, 2, 3)$ for glassy $RAl_{0.30}P_{3.05}O_{9.62}$ obtained by subtracting $S_{RR}(k)$ shown by the solid curve in figure 4 from the $\Delta F^{(i)}_{R}(k)$ shown in figure 3(a) following equation (4). The bars represent the statistical errors on the data points and the solid curves are the back Fourier transforms of the corresponding $\Delta D'^{(i)}_{R\mu}(r)$ after the unphysical low-r oscillations are set to the calculated limit of $-4\pi n_0 r$ (see figure 2). The scaled functions should be identical and the differences between them should therefore be zero within the statistical error.

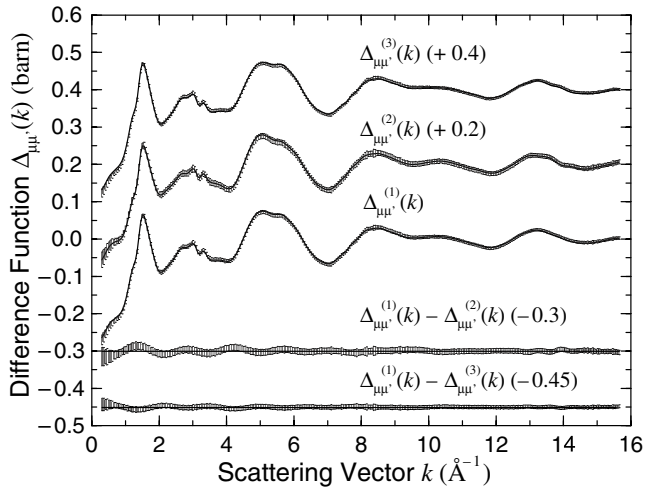

Figure 7. The matrix–matrix atom difference functions $\Delta^{(i)}_{\mu\mu'}(k)$ $(i = 1, 2, 3)$ for glassy $RAl_{0.30}P_{3.05}O_{9.62}$ obtained by subtracting $S_{RR}(k)$ shown by the solid curve in figure 4 from the $\Delta F^{(i)}(k)$ shown in figure 3(b) following equation (6). The bars represent the statistical errors on the data points and the solid curves are the back Fourier transforms of the corresponding $\Delta D'^{(i)}_{\mu\mu'}(r)$ after the unphysical low-r oscillations are set to the calculated limit of $-4\pi n_0 r$ (see figure 2). The functions should be identical on the plotted scale and the differences between them should therefore be zero within the statistical error.

(see figure 5(c)). Two Gaussians were used to represent the first peak, with $\bar{n}^{O_T}_P = 2.32(9)$ at 1.50(1) Å and $\bar{n}^{O_B}_P = 1.68(9)$ at 1.60(1) Å, giving an overall P–O coordination number $\bar{n}^{O}_P = 4.0(1)$. These values for the P–O_T and P–O_B bond lengths are typical of those found

Table 3. Parameters obtained from the Gaussian fit to the $\Delta D'^{(1)}_{\mu\mu'}(r)$ difference function for glassy $RAl_{0.30}P_{3.05}O_{9.62}$.

Correlation (α–β)	$r_{\alpha\beta}$ (Å)	$\bar{n}^{\beta}_{\alpha}$	$\sigma_{\alpha\beta}$ (Å)
P–O_T	1.50(1)	2.32(9)	0.06(1)
P–O_B	1.60(1)	1.68(9)	0.09(1)
Al–O	1.89(2)	5.5(5)	0.12(1)
O–(P)–O	2.45(1)	2.3(1)	0.13(1)
O–(P)–O	2.54(1)	1.4(1)	0.06(1)
O–(Al)–O	2.65(1)	0.7(1)	0.12(1)
P–(OP)–O	2.93(2)	4.0(1)	0.13(1)
P–(O)–P	2.98(2)	2.0(1)	0.10(1)

in other rare-earth phosphate glasses of similar composition [9, 11, 33] and a peak width for P–O_B that is broader than for P–O_T is a typical feature of phosphate glasses [32]. A distance $r_{AlO} = 1.89(2)$ Å was found, in accord with [11, 12], with $\bar{n}^{O}_{Al} = 5.5(5)$. The second peak was fitted with Gaussians centred at 2.45(1), 2.54(1) and 2.65(1) Å corresponding to O–(P)–O coordination numbers of 2.3(1) and 1.4(1) and an O–(Al)–O coordination number of 0.7(1) respectively i.e. the overall O–(P)–O nearest-neighbour coordination number $\bar{n}^{O}_{O} = 3.7(1)$. A single Gaussian fit to the O–(P)–O correlations under the second peak was found to be inadequate, giving a higher R_χ value of 6.2%, and the use of two Gaussians to represent the O–(P)–O correlations was also found to be necessary for R–Al–P–O glasses containing large rare-earth ions [37]. The small peak at 2 Å was found to be mostly an artefact of $M(r)$, the effect of which may be reduced by using a diffractometer which accesses a larger k range. The full set of parameters describing the fitted Gaussians is given in table 3. Within the experimental error, these are the same as the parameters obtained by fitting $\Delta D'^{(2)}_{\mu\mu'}(r)$ and $\Delta D'^{(3)}_{\mu\mu'}(r)$.

5. Discussion

In crystalline and glassy P_2O_5, a network is built from corner-sharing PO_4 tetrahedra comprising one terminal oxygen atom, O_T, and three bridging oxygen atoms, O_B, at distances close to 1.4 and 1.6 Å respectively [6, 62–66]. In the model of Hoppe and co-workers [9, 30–33], the addition of a network modifier such as R_2O_3 leaves the PO_4 tetrahedra intact but depolymerizes the phosphate network through the breakage of P–O_B–P bonds, thereby increasing the fraction of O_T to which the R^{3+} ions are exclusively bound via P–O_T–R linkages. Specifically, if y oxygen atoms from the network modifier are added per P_2O_5 unit, the P:O_B:O_T ratio changes from 2:3:2 in pure P_2O_5 to $2:(3-y):2(1+y)$ in the modified material. The overall O–(P)–O nearest-neighbour coordination number is then given by

$$\bar{n}^{O}_{O} = \frac{(3-y)}{(5+y)}\bar{n}^{O}_{O_B} + \frac{2(1+y)}{(5+y)}\bar{n}^{O}_{O_T} \equiv [\bar{n}^{O}_{O}]_B + [\bar{n}^{O}_{O}]_T \tag{16}$$

where $\bar{n}^{O}_{O_B} = 6$ and $\bar{n}^{O}_{O_T} = 3$ such that $\bar{n}^{O}_{O} = 24/(5+y)$ [31]. In equation (16), $[\bar{n}^{O}_{O}]_B$ and $[\bar{n}^{O}_{O}]_T$ represent the fractional O–(P)–O coordination numbers associated with bridging and terminal oxygen sites respectively. Since P–O_B bonds are longer than P–O_T bonds, the mean O–(P)–O distance associated with the bridging sites is anticipated to be longer than for the terminal sites. The nearest-neighbour P–(O_B)–P coordination number is given by $\bar{n}^{P}_{P} = 3 - y$.

In the case of R–Al–P–O compounds it can be readily shown that $y = 2c_O/c_P - 5$, provided Al acts as a network modifier, and it then follows that the R:O_T ratio is given by $1:2[c_O - 2c_P]/c_R$. When Al is absent, the composition can be written as $(R_2O_3)_x(P_2O_5)_{1-x}$, where x is one-half,

Table 4. Parameters describing the R^{3+} coordination environment in several crystalline rare-earth phosphates. Small R refers to Ho or Er and large R to La or Ce.

R size	Crystal	R–R (min) Å	R:O_T	$\bar{n}_R^{O_T}$	f_s	References
Small	RP_5O_{14}	5.71	8	8	0	[36]
	RP_3O_9	5.37	6	6	0	[35]
	RPO_4	3.75	4	8	1/2	[18]
Large	RP_5O_{14}	5.25	8	8	0	[67]
	RP_3O_9	4.32	6	8	1/4	[68]
	RPO_4	4.10	4	9	5/9	[69]

one-quarter or one-sixth for the ortho-, meta- and ultra-phosphates respectively, in which case $y = 3x/(1-x)$ and the R:O_T ratio becomes $1:(1+2x)/x$ [33]. Hence O–(P)–O coordination numbers, which are in agreement with the observed values for several crystalline R–P–O systems, can be calculated: $\bar{n}_O^O$ is 4.8 for c-P_2O_5 [16, 65, 66], 4.29 for c-RP_5O_{14} [35, 67], 4.0 for c-RP_3O_9 [19, 68] and 3.0 for c-RPO_4 [18, 69]. Furthermore, in the meta- and ultra-phosphate crystalline phases of *small* rare-earth ions, R^{3+} is bound to six or eight O_T respectively, equal to the number of O_T available per rare-earth ion (see table 4). None of the bonded O_T need, therefore, to be shared between the R-centred coordination polyhedra. By contrast, in the meta- and ultra-phosphate crystalline phases of *large* rare-earth ions, R^{3+} is bound to eight O_T in both cases such that 25% of the bonded O_T need to be shared in the case of the metaphosphates.

For glassy $RAl_{0.30}P_{3.05}O_{9.62}$, the Al–O peak position and coordination number suggest that a substantial number of the Al atoms adopt octahedral conformations as in crystalline [60] and glassy [70] AlP_3O_9—i.e. Al_2O_3 appears to act primarily as a network modifier, akin to R_2O_3, from which we deduce $y = 1.320$. Hence we calculate that each P is on average bound to 1.68 O_B and 2.32 O_T with $[\bar{n}_O^O]_B = 1.59$ and $[\bar{n}_O^O]_T = 2.20$, giving an overall O–(P)–O coordination number $\bar{n}_O^O = 3.79$. All of these parameters are in accord with those obtained from the fit to $\Delta D'^{(1)}_{\mu\mu'}(r)$ (see table 3) which implies that the Hoppe *et al* model [9, 30–33] can act as an excellent starting point for understanding the structure of rare-earth phosphate glasses, even when they incorporate a significant mol% of Al impurity atoms.

Furthermore, for sixfold coordinated Al an O_T–(Al)–O_T coordination number of $\bar{n}_O^O = 48c_{Al}/(5+y)c_P = 0.75$ at $\sqrt{2}r_{AlO} = 2.66$ Å is anticipated, while for tetrahedrally coordinated Al a coordination number of $\bar{n}_O^O = 24c_{Al}/(5+y)c_P = 0.37$ at $\sqrt{8/3}r_{AlO} = 2.87$ Å is expected. Thus the available information on the O_T–(Al)–O_T correlations, summarized in table 3, is also consistent with a predominantly octahedral coordination environment for aluminium, the role of which is to bridge PO_4 tetrahedra via O_T–Al–O_T linkages, thereby strengthening [11, 12] the glass network. Small highly charged cations in phosphate glasses are also considered to strengthen the P–O_B–P linkages and form bonds with O_T that are resistant to hydration, thereby enhancing the chemical durability of the glass [71]. It will be interesting to see the extent to which a polarizable, formal charge ionic interaction model can account for the observed phenomena [41–43].

The method of isomorphic substitution in neutron diffraction has also been recently applied to glassy $RAl_{0.35}P_{3.24}O_{10.12}$, where R^{3+} denotes La^{3+} or Ce^{3+} which are at the *large*-cation-radius end of the rare-earth series [37]. The materials were prepared in alumina crucibles and the difference functions $\Delta F_R(k)$ and $\Delta F(k)$ were measured. The glass structure was again found to be based on a network of PO_4 tetrahedra, in which there are on average 2.2(1) O_T at 1.51(1) Å and 1.8(1) O_B at 1.60(1) Å, and the network modifying rare-earth ions bind to a larger number of 7.5(2) O_T in a distribution that is both broad and asymmetric. The overall

results are also consistent with a network modifying role for Al and could be interpreted by using the model of Hoppe and co-workers [9, 30–33]. By reference to the recent ^{27}Al nuclear magnetic resonance (NMR) experiments of Karabulut *et al* [72] on $(M_2O_3)_x(P_2O_5)_{1-x}$ glasses, where M^{3+} is a modifying cation chosen to be La^{3+}, Al^{3+} or a mixture of the two, Martin *et al* [37] developed a model for the Al–O_T coordination number $\bar{n}^O_{Al}$. Specifically, when the O_T bound to Al are not shared between other R- or Al-centred coordination polyhedra (i.e. when Al–O_T–Al or Al–O_T–R linkages do not occur) then

$$\bar{n}^O_{Al} = \frac{2(c_O - 2c_P) - (1 - f_s)c_R\bar{n}^O_R}{c_{Al}} \tag{17}$$

where f_s is the fraction of O_T atoms bonded to R^{3+} that are shared between R-centred coordination polyhedra. If $c_R = 0$, equation (17) reduces to the usual Al–O_T coordination number for Al_2O_3–P_2O_5 glasses when Al–O_T–Al linkages are not formed [73]. When there is no Al present, equation (17) can be solved for f_s to give the expected values summarized in table 4 for the crystalline rare-earth phosphates.

In the case of the present Dy/Ho containing $RAl_{0.30}P_{3.05}O_{9.62}$ glass, $\bar{n}^O_R = 6.7$, $\bar{n}^O_{Al} = 5.5$ and the atomic fractions are $c_R = 0.072$, $c_{Al} = 0.021$, $c_P = 0.218$ and $c_O = 0.689$ whereupon f_s takes on a value of 19%. For this class of R–Al–P–O glasses containing small rare-earth ions, the dependence of $\bar{n}^O_{Al}$ on *composition*, and hence the connectivity parameter f_s, are however unknown. By comparison, Karabulut *et al* [72] studied two series of $(M_2O_3)_x(P_2O_5)_{1-x}$ glasses where the O:P ratio was fixed at 3.0 for series I, corresponding to $x = 0.25$, and at 3.143 for series II, corresponding to $x = 0.30$. The rare-earth cation, La^{3+}, was then systematically replaced by Al^{3+} at fixed total modifier content and the change in the Al–O_T coordination number was measured. For both series, f_s has been deduced [37] and it is found to decrease monotonically to zero as Al^{3+} replaces La^{3+}, most rapidly in the case of series I for which there is a greater number of O_T available per modifying cation, namely 6 compared with 5.33. For both series, the dependence of f_s on the Al–O_T:M–O_T bond ratio, as calculated from the expression $c_{Al}\bar{n}^O_{Al}/(c_R\bar{n}^O_R + c_{Al}\bar{n}^O_{Al})$, is shown in figure 8.

The connectivity parameter, f_s, is of significance when considering the proximity of optically active rare-earth ions which can e.g. be paired, through the formation of R–O_T–R bonded dimers, or otherwise clustered, through the formation of higher-dimensional conformations such as R–O_T–R–O_T–R bonded chains as in a modified random network model [74]. This proximity is important since the mechanism for energy transfer between rare-earth ions has a strong dependence on their separation [75–77]. For example, the clustering of rare-earth ions on the length scale of a few ångstrom can result in cooperative up-conversion processes [78–80] that may have a deleterious effect on the operation of optical devices such as Er-doped fibre amplifiers and lasers [79, 81–83]. On the other hand, efficient energy transfer between a donor (e.g. Yb^{3+}) and acceptor (e.g. Er^{3+}) ion with minimal back-energy transfer is beneficial when making up-conversion lasers [84]. It is therefore desirable to have control of f_s, and hence the sharing of O_T between R^{3+} ions, so that the minimum R–R separation can be set. In the case of the crystalline rare-earth phosphates, this separation is found to be markedly shorter when f_s is finite (see table 4).

For $(M_2O_3)_x(P_2O_5)_{1-x}$ glasses comprising *large* rare-earth ions, f_s can be minimized either by the replacement of La^{3+} by Al^{3+} at fixed total modifier content or by the alteration of x to increase the number of O_T available per network modifying M^{3+} cation (see figure 8). A similar strategy is anticipated to work for *small* rare-earth R_2O_3–Al_2O_3–P_2O_5 glasses, provided that the conditions leading to equation (17) hold, and in this context it would be helpful to have information complementary to that obtained by Karabulut *et al* [72] on the composition dependence of the Al–O_T coordination number.

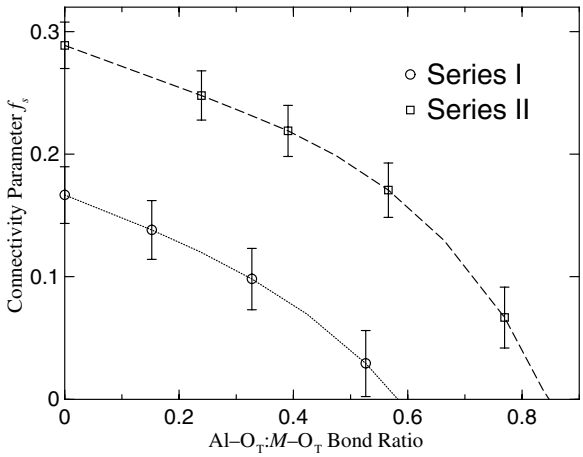

Figure 8. The fraction, f_s, of O_T atoms bonded to large R^{3+} ions that are shared between R-centred coordination polyhedra as calculated from equation (17) for the two series of $(M_2O_3)_x(P_2O_5)_{1-x}$ glasses (M^{3+} = La^{3+} or Al^{3+}) studied by Karabulut *et al* [72], plotted as a function of the Al–O_T:M–O_T bond ratio. The f_s values and Al–O_T:M–O_T bond ratios were deduced using the measured $\bar{n}^{O}_{Al}$ values taken from [72] together with $\bar{n}^{O}_{R}$ values fixed at those obtained experimentally, namely 7.2 (series I) or 7.5 (series II) (see [37]). The *M*:O_T ratio is 6 for series I and 5.33 for series II and the error bars show the effect on f_s of varying the $\bar{n}^{O}_{R}$ values by ± 0.2. The effect of this variation on the Al–O_T:M–O_T bond ratio is smaller than the symbol size.

6. Conclusions

The present work demonstrates that it is possible to identify the R–R correlations in phosphate glasses by using the method of *isomorphic* substitution in neutron diffraction. Furthermore, by taking the Al correlations into explicit account, it is possible to develop a self-consistent model, based on that of Hoppe and co-workers [9, 30–33], for the overall structure of R–Al–P–O glasses comprising *small* rare-earth ions. In the case of glassy $RAl_{0.30}P_{3.05}O_{9.62}$ it is found that a network is formed from corner-sharing PO_4 tetrahedra in which there are, on average, 2.32(9) O_T at 1.50(1) Å and 1.68(9) O_B at 1.60(1) Å. The network modifying rare-earth ions bind to an average of 6.7(1) O_T and are distributed such that 7.9(7) R–R nearest-neighbours reside at 5.62(6) Å, a distance just short of the R–R separation of 5.80 Å expected from a uniform distribution of R^{3+} ions in which their separation is maximized. The Al^{3+} ion also has a network modifying role in which it strengthens the glass through the formation of O_T–Al–O_T linkages. The connectivity of the R-centred coordination polyhedra in R_2O_3–Al_2O_3–P_2O_5 glasses comprising both small and large rare-earth ions is quantified in terms of a parameter f_s. Methods for reducing the clustering of rare-earth ions in these materials are then discussed, based on a reduction of f_s via the replacement of R^{3+} by Al^{3+} at fixed total modifier content or via a change of the M_2O_3:P_2O_5 ratio to increase the number of O_T available per network modifying M^{3+} cation. The present work should provide a new stimulus for the development of realistic microscopic models for glassy rare-earth phosphate materials and the isomorphic approach can be used as an alternative to the method of isotopic substitution in neutron diffraction to identify the relative distribution of rare-earth ions in a variety of other vitreous oxides.

Acknowledgments

It is a pleasure to thank Peter Taylor (Department of Engineering and Applied Science, Bath) for access to furnaces, Hugh Perrott (Centre for Electron Optical Studies, Bath) for the EPMA analysis, and Pierre Palleau (ILL, Grenoble) for help with the neutron diffraction experiments. The financial support of the EPSRC is gratefully acknowledged.

References

[1] Weber M J 1991 *Materials Science and Technology* vol 9, ed J Zarzycki (Weinheim: VCH) p 619
[2] Marion J E and Weber M J 1991 *Eur. J. Solid State Inorg. Chem.* **28** 271
[3] Rapp C F 1995 *CRC Handbook of Laser Science and Technology* (Suppl. 2) ed M J Weber (Boca Raton, FL: CRC Press) p 619
[4] Davey S T, Ainslie B J and Wyatt R 1995 *CRC Handbook of Laser Science and Technology* (Suppl. 2) ed M J Weber (Boca Raton, FL: CRC Press) p 635
[5] Loong C-K, Suzuya K, Price D L, Sales B C and Boatner L A 1998 *Physica* B **241–243** 890
[6] Brow R K 2000 *J. Non-Cryst. Solids* **263/264** 1
[7] Karabulut M, Marasinghe G K, Metwalli E, Wittenauer A K, Brow R K, Booth C H and Shuh D K 2002 *Phys. Rev.* B **65** 104206
[8] Faber T E and Ziman J M 1965 *Phil. Mag.* **11** 153
[9] Hoppe U, Kranold R, Stachel D, Barz A and Hannon A C 1998 *J. Non-Cryst. Solids* **232–234** 44
[10] Mierzejewski A, Saunders G A, Sidek H A A and Bridge B 1988 *J. Non-Cryst. Solids* **104** 323
[11] Cole J M, van Eck E R H, Mountjoy G, Newport R J, Brennan T and Saunders G A 1999 *J. Phys.: Condens. Matter* **11** 9165
[12] Cole J M, van Eck E R H, Mountjoy G, Anderson R, Brennan T, Bushnell-Wye G, Newport R J and Saunders G A 2001 *J. Phys.: Condens. Matter* **13** 4105
[13] Shannon R D 1976 *Acta Crystallogr.* A **32** 751
[14] Pettifor D G 1986 *J. Phys. C: Solid State Phys.* **19** 285
[15] Moeller T 1973 *The Chemistry of the Lanthanides* (Oxford: Pergamon)
[16] Wells A F 1984 *Structural Inorganic Chemistry* 5th edn (Oxford: Clarendon)
[17] Milligan W O, Mullica D F, Beall G W and Boatner L A 1983 *Inorg. Chim. Acta* **70** 133
[18] Ni Y, Hughes J M and Mariano A N 1995 *Am. Mineral.* **80** 21
[19] Hong H Y-P 1974 *Acta Crystallogr.* B **30** 1857
[20] Bagieu-Beucher M and Tranqui D 1970 *Bull. Soc. Fr. Minéral. Cristallogr.* **93** 505
[21] Hong H Y-P and Pierce J W 1974 *Mater. Res. Bull.* **9** 179
[22] Bowron D T, Newport R J, Rainford B D, Saunders G A and Senin H B 1995 *Phys. Rev.* B **51** 5739
[23] Bowron D T, Saunders G A, Newport R J, Rainford B D and Senin H B 1996 *Phys. Rev.* B **53** 5268
[24] Anderson R, Brennan T, Mountjoy G, Newport R J and Saunders G A 1998 *J. Non-Cryst. Solids* **232–234** 286
[25] Anderson R, Brennan T, Cole J M, Mountjoy G, Pickup D M, Newport R J and Saunders G A 1999 *J. Mater. Res.* **14** 4706
[26] Cole J M, Newport R J, Bowron D T, Pettifer R F, Mountjoy G, Brennan T and Saunders G A 2001 *J. Phys.: Condens. Matter* **13** 6659
[27] Mountjoy G, Cole J M, Brennan T, Newport R J, Saunders G A and Wallidge G W 2001 *J. Non-Cryst. Solids* **279** 20
[28] Bowron D T, Bushnell-Wye G, Newport R J, Rainford B D and Saunders G A 1996 *J. Phys.: Condens. Matter* **8** 3337
[29] Cannas M, Manca E, Pinna G, Bettinelli M and Speghini A 1998 *Z. Naturf.* A **53** 919
[30] Hoppe U, Walter G and Stachel D 1990 *Silikattechnik* **41** 227
[31] Hoppe U 1996 *J. Non-Cryst. Solids* **195** 138
[32] Hoppe U, Walter G, Kranold R and Stachel D 2000 *J. Non-Cryst. Solids* **263/264** 29
[33] Hoppe U, Ebendorff-Heidepriem H, Neuefeind J and Bowron D T 2001 *Z. Naturf.* A **56** 237
[34] Martin R A, Salmon P S, Fischer H E and Cuello G J 2003 *Phys. Rev. Lett.* **90** 185501
[35] Dorokhova G I and Karpov O G 1984 *Sov. Phys.—Crystallogr.* **29** 400
[36] Bagieu M, Tordjman I, Durif A and Bassi G 1973 *Cryst. Struct. Commun.* **3** 387
[37] Martin R A, Salmon P S, Benmore C J, Fischer H E and Cuello G J 2003 *Phys. Rev.* B **68** 054203
[38] Wasse J C and Salmon P S 1999 *J. Phys.: Condens. Matter* **11** 1381
[39] Yarnell J L, Katz M J, Wenzel R G and Koenig S H 1973 *Phys. Rev.* A **7** 2130

[40] Wasse J C, Salmon P S and Delaplane R G 2000 *J. Phys.: Condens. Matter* **12** 9539
[41] Hutchinson F, Rowley A J, Walters M K, Wilson M, Madden P A, Wasse J C and Salmon P S 1999 *J. Chem. Phys.* **111** 2028
[42] Hutchinson F, Wilson M and Madden P A 2000 *J. Phys.: Condens. Matter* **12** 10389
[43] Hutchinson F, Wilson M and Madden P A 2001 *Mol. Phys.* **99** 811
[44] Penfold I T and Salmon P S 1990 *Phys. Rev. Lett.* **64** 2164
[45] Salmon P S, Xin S and Fischer H E 1998 *Phys. Rev.* B **58** 6115
[46] Benmore C J and Salmon P S 1994 *Phys. Rev. Lett.* **73** 264
[47] Liu J and Salmon P S 1997 *Europhys. Lett.* **39** 521
[48] Salmon P S and Xin S 2002 *Phys. Rev.* B **65** 064202
[49] Martin R A 2002 *PhD Thesis* University of Bath, unpublished
[50] Fischer H E, Palleau P and Feltin D 2000 *Physica* B **276–278** 93
[51] Fischer H E, Cuello G J, Palleau P, Feltin D, Barnes A C, Badyal Y S and Simonson J M 2002 *Appl. Phys.* A **74** S160
[52] Bertagnolli H, Chieux P and Zeidler M D 1976 *Mol. Phys.* **32** 759
[53] Jal J F, Mathieu C, Chieux P and Dupuy J 1990 *Phil. Mag.* B **62** 351
[54] Sears V F 1992 *Neutron News* **3** 26
[55] Lynn J E and Seeger P A 1990 *At. Data Nucl. Data Tables* **44** 191
[56] Cossy C, Barnes A C, Enderby J E and Merbach A E 1989 *J. Chem. Phys.* **90** 3254
[57] Mughabghab S F 1984 *Neutron Cross Sections* part B, vol 1 (Orlando, FL: Academic)
[58] Soper A K, Andreani C and Nardone M 1993 *Phys. Rev.* E **47** 2598
[59] Grimley D I, Wright A C and Sinclair R N 1990 *J. Non-Cryst. Solids* **119** 49
[60] van der Meer H 1976 *Acta Crystallogr.* B **32** 2423
[61] Hannon A C and Parker J M 2000 *J. Non-Cryst. Solids* **274** 102
[62] Hoppe U, Walter G, Barz A, Stachel D and Hannon A C 1998 *J. Phys.: Condens. Matter* **10** 261
[63] Hoppe U, Walter G, Kranold R and Stachel D 1998 *Z. Naturf.* A **53** 93
[64] Hoppe U, Kranold R, Barz A, Stachel D and Neuefeind J 2000 *Solid State Commun.* **115** 559
[65] Stachel D, Svoboda I and Fuess H 1995 *Acta Crystallogr.* C **51** 1049
[66] Arbib E H, Elouadi B, Chaminade J P and Darriet J 1996 *J. Solid State Chem.* **127** 350
[67] Cole J M, Lees M R, Howard J A K, Newport R J, Saunders G A and Schönherr E 2000 *J. Solid State Chem.* **150** 377
[68] Matuszewski J, Kropiwnicka J and Znamierowska T 1988 *J. Solid State Chem.* **75** 285
[69] Beall G W, Boatner L A, Mullica D F and Milligan W O 1981 *J. Inorg. Nucl. Chem.* **43** 101
[70] Hoppe U, Walter G, Stachel D and Hannon A C 1995 *Z. Naturf.* A **50** 684
[71] Metwalli E and Brow R K 2001 *J. Non-Cryst. Solids* **289** 113
[72] Karabulut M, Metwalli E and Brow R K 2001 *J. Non-Cryst. Solids* **283** 211
[73] Brow R K, Click C A and Alam T M 2000 *J. Non-Cryst. Solids* **274** 9
[74] Greaves G N 1985 *J. Non-Cryst. Solids* **71** 203
[75] Auzel F E 1973 *Proc. IEEE* **61** 758
[76] Wright J C 1976 *Radiationless Processes in Molecules and Crystals* ed F K Fong (Berlin: Springer) p 239
[77] Blasse G 1979 *Handbook on the Physics and Chemistry of Rare Earths* vol 4, ed K A Gschneidner Jr and L Eyring (Amsterdam: North-Holland) p 237
[78] Barthem R B, Buisson R, Madèore F, Vial J C and Chaminade J P 1987 *J. Physique* **48** 379
[79] Delevaque E, Georges T, Monerie M, Lamouler P and Bayon J-F 1993 *IEEE Photonics Technol. Lett.* **5** 73
[80] Auzel F, Meichenin D, Pellé F and Goldner P 1994 *Opt. Mater.* **4** 35
[81] Blixt P, Nilsson J, Carlnäs T and Jaskorzynska B 1991 *IEEE Trans. Photonics Technol. Lett.* **3** 996
[82] Wagener J L, Wysocki P F, Digonnet M J F and Shaw H J 1993 *Opt. Lett.* **18** 2014
[83] Wagener J L, Wysocki P F, Digonnet M J F and Shaw H J 1994 *Opt. Lett.* **19** 347
[84] Hwang B-C, Jiang S, Luo T, Watson J, Sorbello G and Peyghambarian N 2000 *J. Opt. Soc. Am.* B **17** 833